Initiation of electrical discharge at the triple junction of the lightning protection of an aircraft radome

F. Padoan[1], D. Clark[1], A. Haddad[1], C. Karch[2], P. Westphal[2]

[1]Morgan-Botti Lightning Laboratory, Advanced High Voltage Engineering Research Centre, School of Engineering, Cardiff University, CF24 3AA, UK
[2]Cross Domain System Engineering – TEYYX Airbus Defence and Space GmbH, Rechliner Straße, 85077 Manching, Germany

Key words: aircraft radome, lightning protection, numerical simulations, triple junction point, lightning testing.

HEADLINE

This article highlights challenges in aircraft design focusing on lightning protection of an aircraft radome. A Multiphysics analysis is performed in conjunction with various laboratory high voltage test configurations, and the effects of high temperature and pressure are discussed.

INTRODUCTION

The radar antenna in aerospace applications is often located at the front end of the aircraft. To allow communications and transparency to the high frequency electromagnetic waves, the radar antenna is housed within an insulating dome, commonly known as the radome. As such, lightning strikes can easily hit the radar antenna despite being inside the radome as the latter has very little electric field shielding capability due to its dielectric material property.

To offer satisfactory shielding against lightning strikes while allowing electromagnetic waves through to and from the antenna, the radome is protected using metal diverter strips spread around the radome surface (Figure 1). In some other applications, segmented strips were used, each consisting of a series of metal electrodes fixed onto a strip of resistive material, as shown in Figure 2. During a discharge, the gap between the metal electrodes ionizes and provides a plasma channel in which the lightning current can be diverted to the fuselage.

These protective devices are now widely tested and used on civilian and military aircraft [1-4], which fulfills requirements of both lightning protection and transparency to the radar's electromagnetic communication signals.

When the aircraft approaches thunderclouds, the elevated electric fields surrounding the radome area often generate coronas and electrical arcing under lightning strike conditions.

In most aerospace applications, the solid bar or metal foils strips are attached to the external surface of the radome [5], and they extend from the fuselage to approximately two thirds of the radome height. Using this configuration, a streamer-leader inception is more likely initiated from the tip of these strips, instead of the antenna.

To predict locations of highest field magnitudes, hence prospective discharge initiation sites, the numerical simulations revealed a spike in the electrical field magnitude close to the triple junction point (TJP) formed at meeting location of the strips ends, dielectric material of the radome, and the air [6]. Depending on the atmospheric and materials surface conditions, this high field magnitude may initiate air ionization, streamer propagation and/or undesirable onerous puncture of the radome wall if the dielectric strength of the radome material is exceeded.

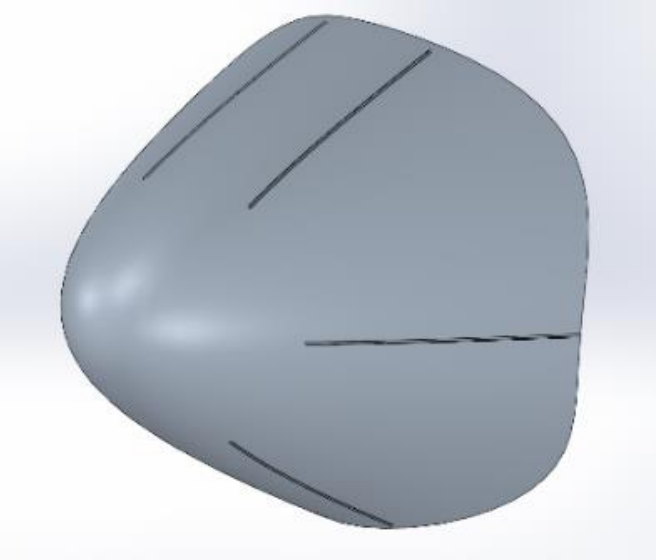

Figure 1: Typical spatial distribution and number of solid diverter strips on a commercial radome geometry.

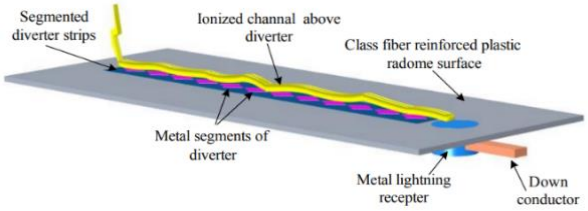

Figure 2: Lightning plasma channel on the segmented diverter strip [4].

It is proposed that the numerical field computations can be exploited to predict and optimize the are where the discharge might occur, while considering the antenna pattern at the same time. In this work, numerical field simulations were performed using COMSOL Multiphysics to study a standard recommended laboratory high voltage test configuration. In this set up, various voltage shapes are applied to a high voltage electrode pointing in the direction of a test radome equipped with solid diverter strips. Different spatial diverter strip arrangements were studied to study the shielding effect and, where possible, determine the possible location points of lightning attachment.

In this work, a further study using magneto-hydrodynamics equations was undertaken to evaluate the generated high temperatures and pressures after the lightning strike channel is formed. These investigations have revealed very high temperatures close to the lightning strike impact area, High temperature can trigger irreversible changes to the properties of the radome material, and it can drive a thermally induced dielectric breakdown of the radome material in extreme cases.

To validate the numerical results, laboratory tests were undertaken in the High Voltage Laboratory at Cardiff University. A radome of a commercial aircraft was tested under a high electric field generated by a high voltage DC applied to a sphere electrode. This test campaign allowed comparison of measured and simulated voltages that cause discharge initiation.

STANDARD RECOMMENDATIONS FOR TESTING RADOME LIGHTNING PROTECTION

Lightning protection of aircraft relies on modeling, but it is also mandatory to carry out representative laboratory tests to demonstrate safety and compliance. Testing with natural lightning in flight carries too much risk for the crew and aircraft and cannot be modified to suit any specific test conditions. Carefully controlled tests on full aircraft with both voltage and current magnitudes of lightning strikes are not possible in the laboratory. Therefore, high current tests up to 200kA are conducted with relatively low voltage magnitudes of few tens of kilovolts are used to evaluate the conduction withstand properties of materials and components. On the other hand, high voltage tests up to megavolts are adopted to evaluate insulation and discharge characteristics of devices and structures; the current in such tests is limited and has no consequences on the test outcomes.

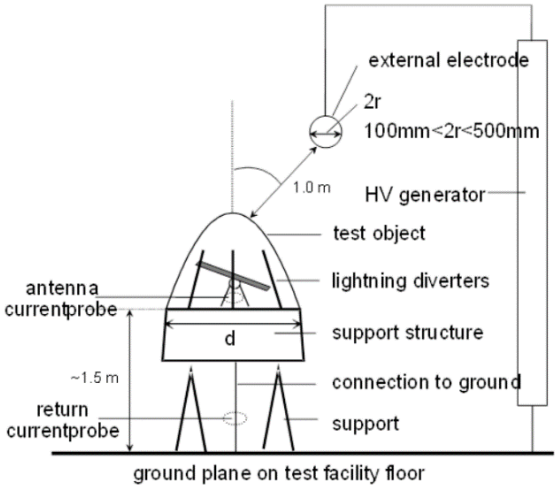

Figure 3: Modified laboratory setup for radome lightning protection tests according to EUROCAE ED-105A [7].

Aerospace standards, such as EUROCAE ED-105A [7], recommend specific models and laboratory test set ups to evaluate the lightning protection efficacy of new protection designs for radomes. Figure 3 reproduces the modified initial leader attachment test setup for testing the radome lightning protection system.

OVERVIEW OF PREVIOUS MODELING WORK OF RADOME LIGHTNING PROTECTION SYSTEM

To determine the electric field distribution and magnitude at various locations of the radome systems and its lightning protection system, several analytical and numerical approaches have been developed.

The laboratory configuration adopting various diverter strip geometries was simulated and the electric field evaluated for different scenarios of radomes. Such work revealed changes in the surface charge distribution for different applied voltage waveshapes.

Another model [4] uses electrostatic field computations on a diverter strip fixed onto a flat sample of dielectric material. In this case, variations in the antenna gain were quantified when the diverter strips were relocated to different position on the radome surface.

The analytical solution developed in [8] demonstrated that the electric field inside the radome volume can reach very high values. The authors used a simple geometry and a constant applied electric field. The investigation revealed that leaders can initiate from the aircraft if the magnitude of the applied ambient field is within the critical range of $E_{cr} \approx 50\ to\ 80\ kV/m$. This range corresponds to the measured fields within a thunderstorm cloud.

The authors in [5], investigated the role the geometry and configuration of segmented diverter strips play in the electric field distribution under lightning strike conditions. For this, models with and without diverter strips were simulated to study and compare the breakdown conditions for the test gap. This work has also proposed that the segmented strip can be modelled as short conductors connected in series with gaps and exhibiting stray capacitances to the airframe of the aircraft.

A magnetohydrodynamic (MHD) model was implemented in [9] to seek the best design of segmented diverter strips to encourage and enhance better discharge process after the positive and negative leaders have connected, and the return stroke is started.

Related work to the study of lightning protection of radomes focussed on investigations to clarify the interaction between the long spark gap and the radome and the aircraft. These have helped improved understanding of the attachment physics [10-12] and the phenomenon of charge accumulation in a cumulonimbus cloud [13].

In this article, we use the finite element method to investigate key characteristics of the lightning discharge on the radome and its lightning protection diverter strips. First, commercial software solving Maxwell's equations was utilised to determine electric field magnitudes around the prospective attachment point, particularly at the triple junction point. The resulting temperature and pressure changes following such lightning strikes were also evaluated to assess potential damage to the radome material and structure.

MODELING THE RADOME AND DIVERTER STRIPS

Attachment point evaluation

The setup shown in Figure 3 is modeled, and numerical computations of electric field and charge distribution are performed. Both the dielectric surface of the radome and the metal diverter strips were included in the model. In particular, the solution results at the points of highest field magnitudes, which are located at the interface between the metal, dielectric and air. The highest magnitude is located closer to the tip of the diverter strip. This triple junction point is the location where electrical discharges can be initiated.

The standard test voltage waveforms B and D with both polarities were used in the simulations and applied to the high voltage electrode. The waveforms are particularly useful to generate impulsive field magnitudes sufficient to initiate streamers but below the flashover of the gap between the HV electrode and the radome.

Waveform B is characterized with a fast front of the order of few microseconds and is known to result in less attachment points, located at the high field sites. However, it has a high probability to produce a dielectric puncture of the dielectric material. In contrast, waveform D, which is characterized by a slow front of few hundred microseconds, results in a variety of attachment points, including to lower electric field regions [14]. Experiences with laboratory testing [15] and in-flight data collection under lightning conditions [16] have helped in setting up optimized conditions for testing.

Radome and diverter strips dimensions

SolidWorks was used to create the radome geometry and associated energization electrode. Real life dimensions

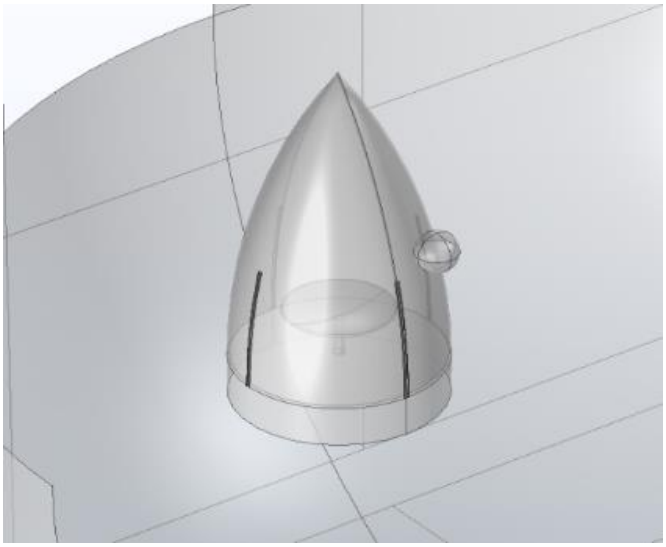

Figure 4: Radome geometry imported into COMSOL Multiphysics. The external spherical domain and the electrode were added in COMSOL.

of aircraft radome were used. The inner height of the tangent ogive radome is $L_{in} = 1.504$ m and the inner base radius is $R_{in} = 0.475\,m$. The inner ogive radius is $\rho_{in} = 2.6186\,m$.

These dimensions allowed the generation of a model for a monolithic radome having a thickness of 10.013 mm. The supporting structure together with a parabolic antenna were built using the following dimensions: $D - d/D = 0.05$, where D is antenna diameter of $D = 0.5\,m$, d is antenna height of $d = 0.225\,m$. The supporting base has a diameter of 0.97 m and a height of 0.20 m. The diverter strips were added on the radome outer surface using an extruded cut of 5 mm in the surface. The adopted strip height is 0.80 m and its width is 0.02 m. Once the geometry had been finalized in SolidWorks, it was then imported into COMSOL Multiphysics for further refinement and processing. Figure 4 shows the resulting model of the radome and diverter strips. The radome structure is surrounded with a spherical computation domain having a radius r=3m. A small sphere located at a distance r=0.1m from the radome was added so that the high voltage waveform could be assigned to it

Material selection

For the simulations, the radome was assumed to be made of fiberglass having a relative permittivity $\varepsilon_r = 3.3$ and a very low conductivity of $0.0001\,S/m$.

The top antistatic paint layer, which is added in the Physics processing section is shown as a Boundary condition to avoid meshing problems.

Copper was used as material for the remaining parts, radome base, antenna and strips. As this study considers only electric field distribution and is not concerned with current flows, the material for the metals is not so crucial. However, high conductivity is required to ensure formation of a single equipotential and redistribution of charges.

The other regions of the model are assumed as air.

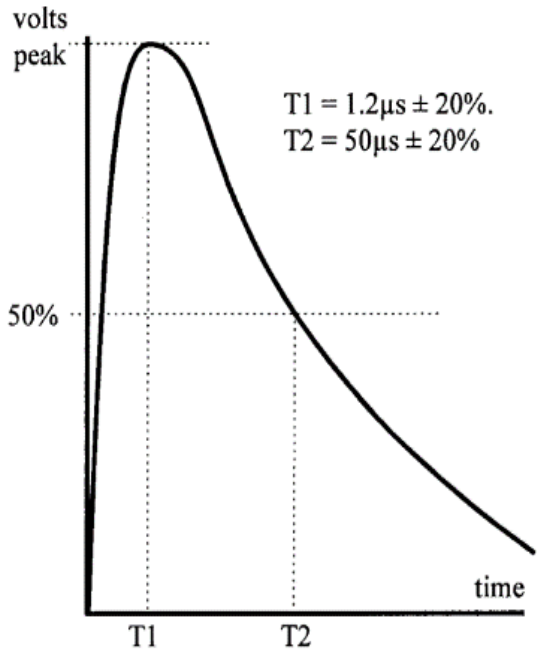

Figure 5: Voltage waveform B as described in [14], T_1=1.2μs and T_2=50μs.

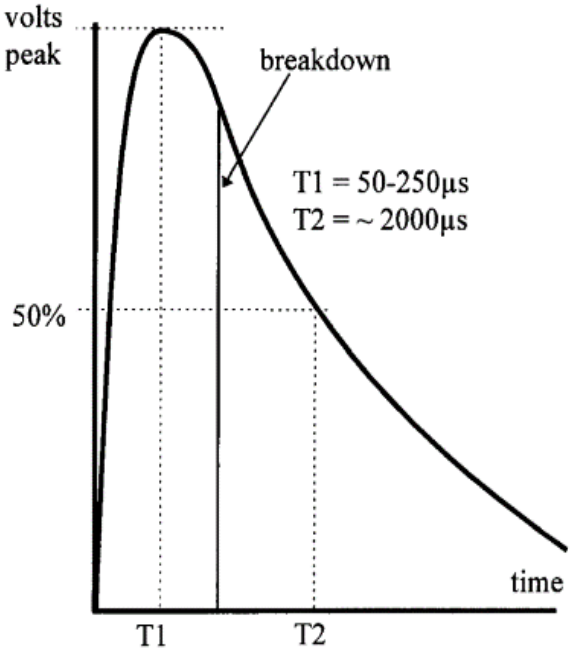

Figure 6: Voltage waveform D as described in [14]. T_1 between 50 and 250μs and T_2=2000μs

Physics and Boundary Conditions

For this simulation, a voltage waveform B, as depicted in Figure 5, is applied to the spherical electrode using a double exponential shape with a peak voltage 1 MV. Its equation is defined as follows:

$$V = 1050 \cdot \left(e^{-\frac{t}{70[\mu s]}} - e^{-\frac{t}{0.40[\mu s]}} \right) [kV] \qquad (1)$$

To evaluate charge distribution, a longer impulse time consisting of voltage waveform D (Figure 6), and having peak value of 1 MV was applied to the spherical electrode:

$$V = 1050 \cdot \left(e^{-\frac{t}{2000[\mu s]}} - e^{-\frac{t}{20[\mu s]}} \right) [kV] \qquad (2)$$

The radome base, the diverter strips and the antenna surface were assigned a ground boundary condition ($V = 0\ V$).

An "electric shielding" boundary condition is imposed on the outer radome surface, with

$$n \cdot (J_1 - J_2) = -\nabla \cdot d_s(\sigma \nabla V) \qquad (3)$$

Where d_s is the layer thickness, J_1 and J_2 are the current densities in air and antistatic paint, respectively.

Mesh refinement

A user-defined mesh was selected. The final built mesh had 945,259 domain elements, 156,879 boundary elements and 10,738 edge elements. This allows one to obtain a complete and sufficient resolution of the numerical solution.

The mesh was further refined around the end of the diverter strip (Figure 7) and at the radar antenna, which enhances the accuracy of the simulation.

Simulation Results

The previously described two voltage waveforms have been applied to the HV electrode. The simulations were considered for various scenarios: a) radome, base and antenna without the diverter strips, b) radome and diverter strips, and c) by adding the antistatic paint layer. Waveform B was applied the HV spherical electrode, and the accumulated charge and the maximum electric field on the antenna were computed.

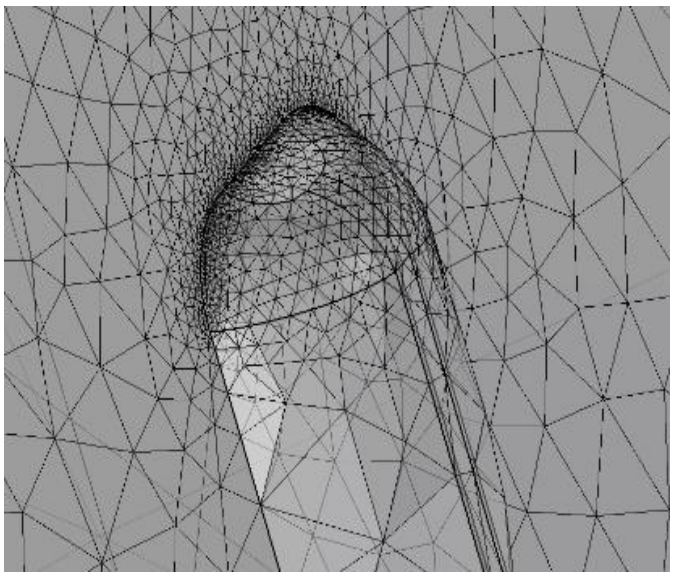

Figure 7: Refined mesh around end of diverter strip.

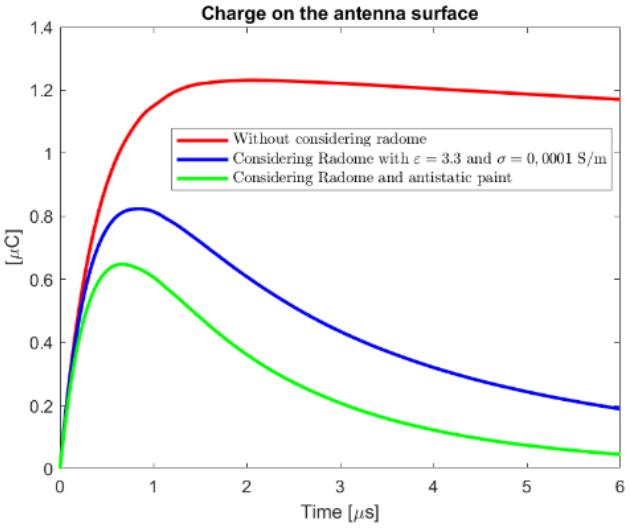

Figure 8: Total charge accumulation on antenna surface, with Voltage Waveform B.

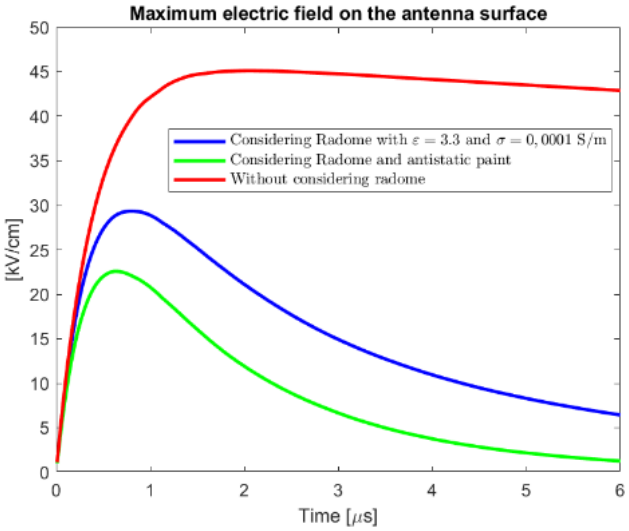

Figure 9: Maximum electric field on the antenna surface, imposing voltage wave B.

As can be seen on Figure 8, the accumulated charge on the antenna surface decreases with the introduction of the radome and diverter strips, and then further decreases when the electrostatic paint was added. A similar observation can be made on the maximum electric field on the antenna surface. The beneficial shielding effects of the diverter strips and electrostatic paint are very clearly exhibited on Figure 9. It is worth noting that similar trends were obtained in [2].

The magnitude of the accumulated charge without the presence of the diverter strips is sufficiently high to initiate a discharge from the antenna edges. This can also be seen in Figure 9 where the field magnitude is in excess of strength value of 30 kV/cm, which is the threshold for air ionization under normal atmospheric conditions. At altitude, both pressure and temperature are lower than at sea level, which will lead to initiation of discharge at lower field magnitudes.

With voltage waveform D, the shielding effect of the strips and antistatic paint are clearly more effective reducing charge and field to very low magnitudes. Figures 10 and 11 show the computed accumulated charge and electric field at the antenna surface.

One of the key features of the computed electric field on the surface of the radome in this simulation is the electric field magnitude spike in the vicinity of the triple junction point, as clearly illustrated in Figures 12 and 13. As can be seen, the magnitude of the electric field increases sharply near the triple junction point to reach a value in excess of 30kV/cm.

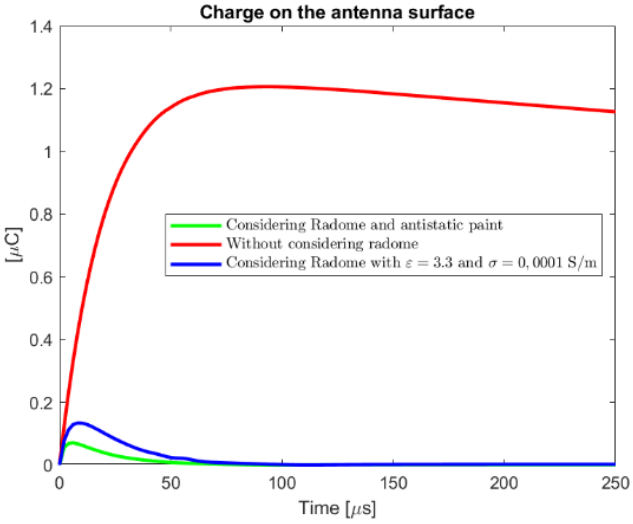

Figure 10: Total charge accumulation on antenna surface, considering, Voltage Wave D.

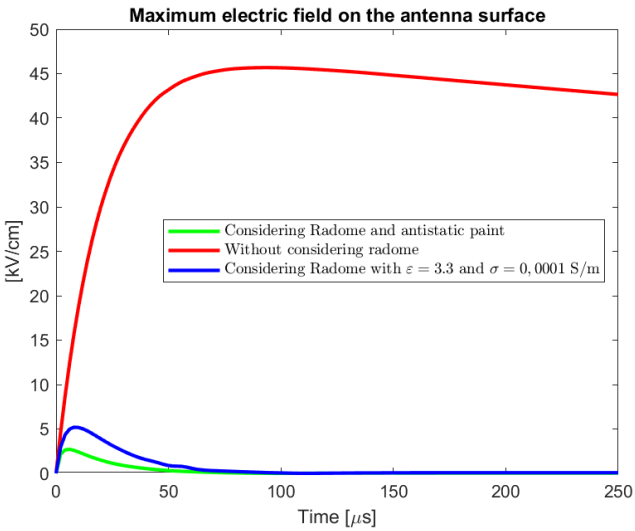

Figure 11: Maximum electric field at the antenna surface imposing voltage wave D.

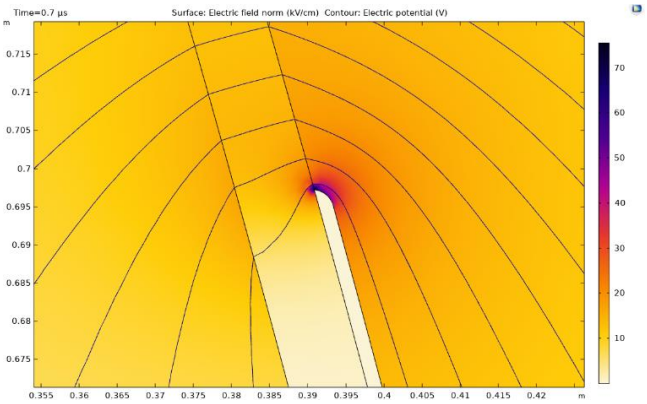

Figure 12: 2D equipotential lines on a close up at the diverter strip end.

The high field magnitude also appears in the radome material. Such fast changing high field can lead to dielectric breakdown of the radome material, causing the so-called "radome pinhole puncture".

To assess this problem of high electric field, different strip geometries have been studied in this work. These include:

- twin diverter strips arrangement with one strip fixed on the outer surface of the radome and the other on the inner surface directly facing the outer one. This arrangement comparatively reduces the electric field around the single strip.
- diverter strips on the internal surface of the radome fastened with screws pointing to the outer surface of the radome. The principle of this design relies on the conducting screws intercepting the lightning strike and diverting the strike current to the internal diverter strip. In this way, it is postulated that the radome puncture will be avoided. A further advantage of this design is its better aerodynamic performance.

These innovative mitigation techniques for the triple junction point undesirable high field magnitude reduce the field magnitude but may lead to high current flows and hence heating effects on the radome material. Furthermore, the electric field magnitude is now high inside the radome, and this could lead to an internal arc from the internal diverter strip and the radar antenna.

MHD MODELLING AND TEMPERATURE EFFECTS

Considering the computed fields around the diverter strip edges, electrical discharges may be initiated under elevated ambient fields. Once the discharge is initiated, the electric field and current flow condition can be high enough to cause damage due to extreme temperatures and pressures in that small area of the triple junction.

Assuming that the lightning channel is just being established when the discharge initiated at the aircraft connects with the leader from the cloud, a study using a thermal plasma can conducted.

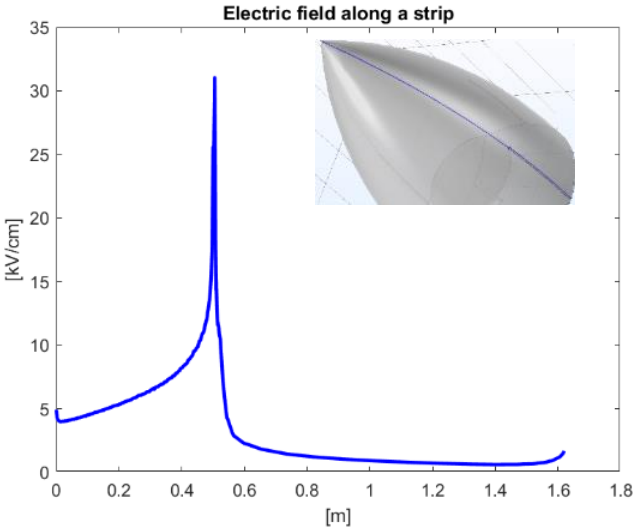

Figure 13: Electric field magnitude along the diverter strip next to the HV electrode and the path of field computation is shown in the COMSOL model shape.

Considering a pressure of 1 bar and a temperature of $T > 10\ 000\ °C$, and assuming that the electrons and heavy particles have the same average speed with many collisions, we can represent the plasma in this case as a "conductive fluid", which then validates the use of the Magnetohydrodynamic equations as replicated here.

$$\frac{\partial \rho}{\partial t} + \nabla \cdot \rho V = 0 \quad (4)$$

$$\frac{d\rho V}{dt} = -\nabla p - \frac{1}{c} J \times B \quad (5)$$

$$E + \frac{V \times B}{c} = \eta J \quad (6)$$

$$\nabla \cdot E = \frac{\rho_c}{\varepsilon_0} \quad (7)$$

$$\nabla \cdot B = 0 \quad (8)$$

$$\nabla \wedge E = -\frac{\partial B}{\partial t} \quad (9)$$

$$\nabla \wedge B = \frac{j_s}{\varepsilon_0 c^2} + \frac{1}{c^2}\frac{\partial E}{\partial t} \quad (10)$$

Where ρ is the mass density $[kg/m^3]$, V is the local mean velocity of particles $[m/s]$, J is the current density $[A/m^2]$, ρ_c is the charge density $[C/m^3]$, B is the magnetic field [T], E is the electric field [V/m], ε_o is the dielectric constant in vacuum.

Further assumptions are required for the MHD model including stationary arc, plasma as a single weakly compressible Newtonian fluid (Argon at local thermodynamic equilibrium), and Lorentz forces treated as laminar flow. For these simulations, gravity effects are neglected, and atmospheric pressure is used.

Previous simulation work [17-24] reported the temperature and pressure conditions on the fuselage of an aircraft. These studies used a discharge between an electrode and a copper plate, with a gap from 3 mm to 50 mm.

MHD computation model

The 2D geometry setup consists of a tungsten cathode and a plain aluminum anode with a gap of 10 mm filled with argon. This configuration was used to investigate the discharge conditions impact on the conductive components, evaluating the temperature and pressure limit values for the relevant mechanical and thermal integrity studies.

Physics and Boundary conditions

The software allows coupling of the electric current, magnetic field, laminar flow, and heat transfer. The following settings were adopted for the various computation modules:

(1) Electric current: to speed up the solution, a linear discretization was adopted. The anode is grounded while a normal current density was applied at the cathode of the model (tip of energized electrode). The current density, J, is assumed to decrease radially (r), as

$$J_z(r) = J_{max} e^{-br} \quad (11)$$

With $b = 1{,}364.54\ (1/m)$, we obtain $J_{max} = 1.2 \cdot 10^8\ A/mm^2$. The current is defined from

$$I = 2\pi \int_0^{R_c} J(r)dr \quad (12)$$

with R_c beingthe cathode radius. For this study, a peak current magnitude of I = 200A was used.

(2) A magnetic field was assumed perpendicular to the computation plane.

(3) A 300K temperature was set in the argon domain and 1,000K set at its boundary. The Boundary heat source set to the electrodes in order to have the radiation cooling from the solid to the gas. The plasma channel had an initial temperature of 10,000K.

(4) To reduce computation time, a weakly compressible flow was used for laminar flow. Also, an open boundary was adopted.

Computation results from plasma simulation

After the arc is formed between the tungsten electrode and the plane anode, the temperature condition in the gas increases fast up to 20,000K. For the radome, such high temperature can cause significant irreversible damage to the materials.

The results for this numerical model were compared with those in [17] and [18]. In [17], good agreement is reported for temperature distribution (Figure 14.a). Figures 14.b and 14.c were obtained for similar geometries and dimensions but with the Cardiff model in Figure 14.c having rounded edges on the cathode.

As can be observed in Figure 14, the isothermal lines obtained with the three independent studies show comparable distributions, with a maximum temperature value of 21,000K in [17], 21,700 K in [18] and 23,700K in the present work.

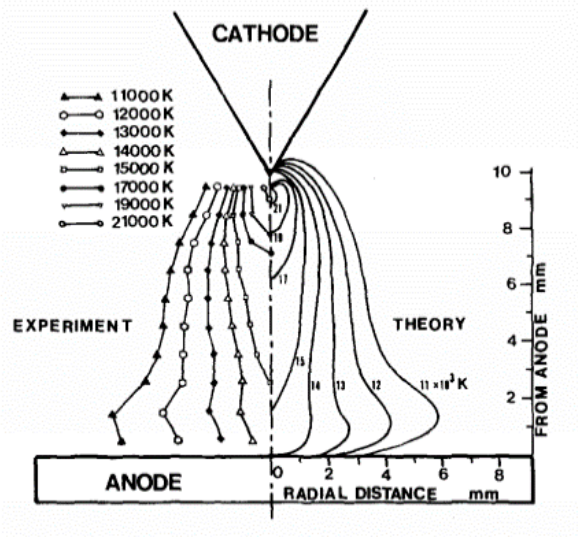

(a)

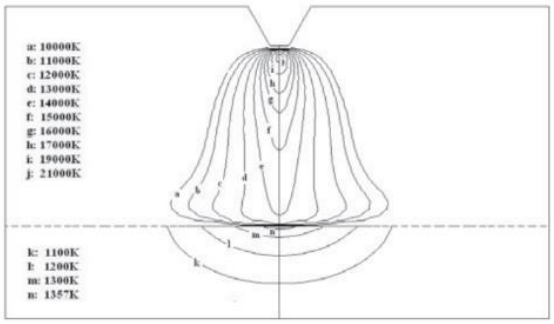

(b)

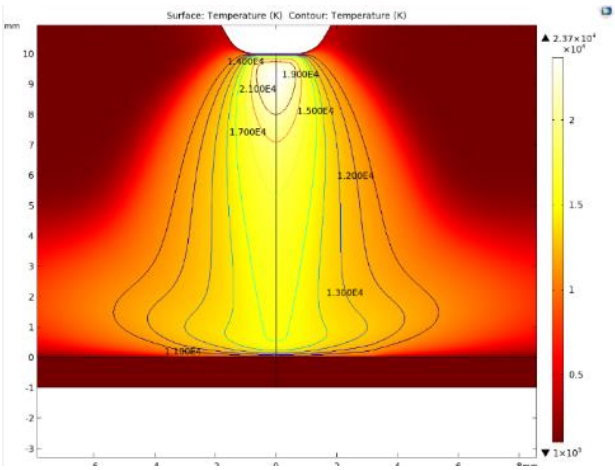

(c)

Figure 14: 2D Temperature distribution between the cathode and the aluminum plate anode. Results: (a) [17], (b) [18], and (c) Cardiff model

The variations of the velocity in the axial direction indicate good agreement between the various simulations, as illustrated in Figure 15.

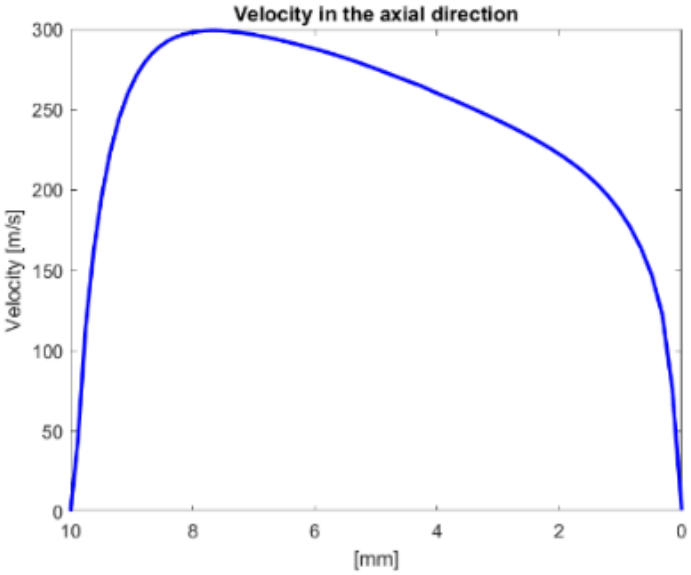

(a)

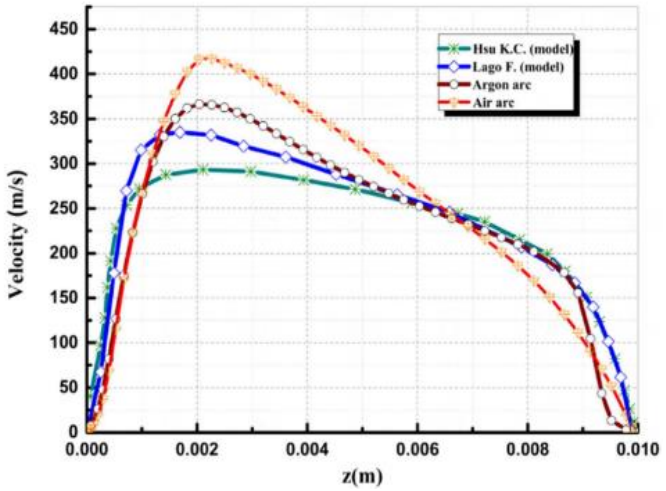

(b)

Figure 15: Velocity variations in the axial direction obtained (a) in this work and (b)by others [20].

LABORATORY MEASUREMENTS

A laboratory test was performed on a Boeing 737 aircraft radome to determine and verify the model for the inception location in a radome structure. A high voltage electrode located close to the radome, as shown in Figure 16, was energized with a positive polarity voltage of magnitude up to 100kV DC. In this way, an increasing high electric field is generated with increasing applied voltage until discharge initiation at the tip of the diverter strip is obtained.

Laboratory setup

The adopted test circuit in this work is shown in Figure 17. An HVDC generator (LH Open Stack Series), capable of delivering up to 100kV positive or negative polarity was used to energize a 25 cm diameter spherical electrode fixed close to the radome, directly facing one of the diverter strips (as seen in Figure 16). The spherical electrode can be moved both vertically and horizontally to test different configurations.

Figure 16: Laboratory setup.

The diverter strip closest to the energized spherical electrode is grounded separately from the others to measure current flow through it. The others were connected together and grounded separately. Shunt resistors were used to measure the current flow to ground from the various grounded points. A resistive divider was used to measure the voltage.

During the tests, a daylight UV camera (COROCAM) was used to detect the very early faint discharges, which are not visible to the naked eye. Such detection system allows location of the source of the discharge.

Before testing, a simulation of the test geometry was performed on various scenarios to compute electric field and estimate the required spacing of the sphere electrode from the diverter strip. An example of such simulation is shown in Figures 18 and 19.

Test procedure and results

In this test program, a number of HV electrode positions were evaluated. The initial test did not show any discharge activity for voltage levels and electrode spacings. It was quickly realized that the antistatic paint prevented such activity. Removing the paint around a small area in the vicinity of the diverter strip end allowed observation of discharge activity for a gap of 10cm, as shown in the example of Figure 20 which shows a peak of 5mA at an applied voltage of 80kV.

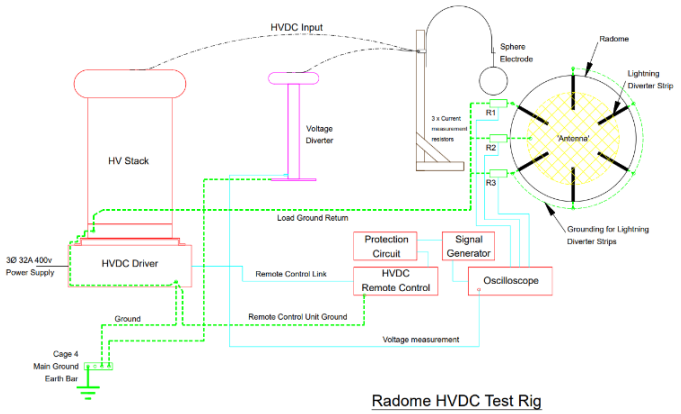

Figure 17: Laboratory setup to evaluate the inception point on a Boeing-747 Radome.

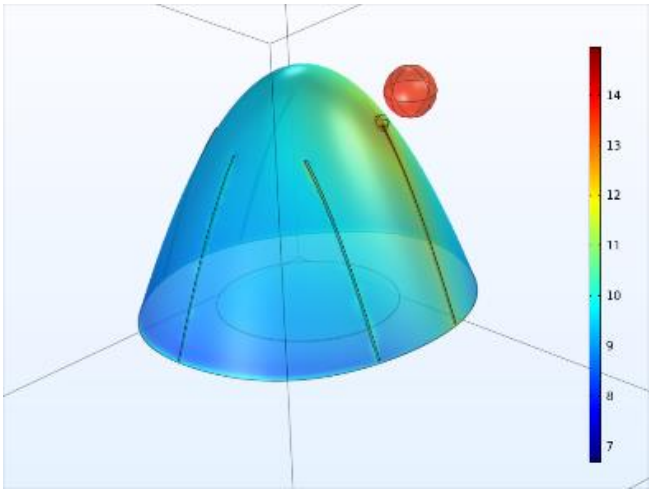

Figure 18: Computed electric field on the radome surface, applied voltage V=100 kV.

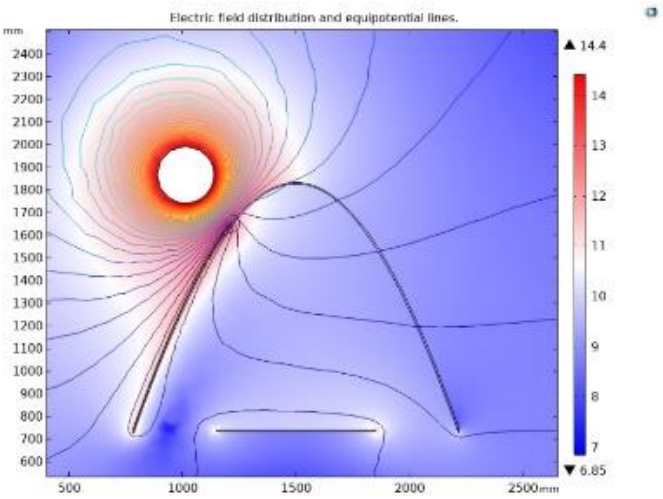

Figure 19: 2D Equipotential lines distribution

.

After some extended activity at an elevated voltage of 100kV and a flashover of the gap, clear degradation can be seen at the triple junction point on the surface of the diverter strip, as reported in Figure 21. It should be highlighted that the magnitudes of discharge currents and the current during flashover are much lower than those expected during lightning strikes. This may imply that more severe erosion would be expected during the high current phase of a lightning strike..

DISCUSSION AND CONCLUSIONS

The diverter strips sued for lightning protection used for aircraft radome have been investigated to determine their efficacy and performance.

It was demonstrated that the presence of the solid diverter strips significantly reduces the electric field magnitude at the radar antenna located within the radome, hence preventing initiation of discharge from the antenna under lightning electric fields conditions.

Simulation of the recommended standard configuration and associated applied waveshapes quantified the charge and electric magnitudes and their distributions. Whilst the field magnitude is significantly reduced at the antenna surface, it was found that a spike in the electric field magnitude is clearly observable at the triple junction point, where the diverter strip end meets the radome material and air. Such elevated field could initiate the electrical discharge under lightning conditions.

Furthermore, the high filed may explain the observed "pinhole puncture" seen on radomes struck by natural lightning. In the light of this work, it is suggested that the high field at the triple junction point may exceed the dielectric strength of the radome material and cause its puncture

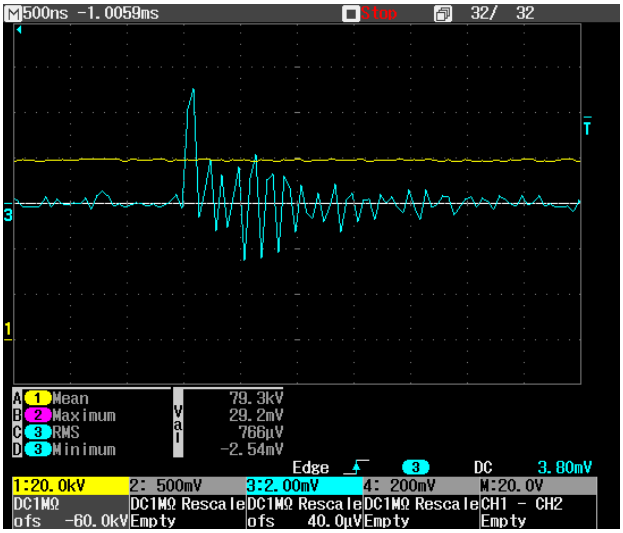

Figure 20: Example of recorded partial discharge activity for a 10cm gap.

Figure 21: Eroded diverter strip end due to discharge activity and flashover. The yellow material is the dielectric material underneath the antistatic paint and the black regions show the metal erosion at the attachment point of flashover event.

A plasma simulation model was developed to examine the temperatures generated after the lightning channel is established and the return stroke current starts to flow. Under such conditions temperatures as high as 21,000K were predicted. These results were in agreement with other independently predicted results.

A laboratory test set up was developed to compare computation and measurement results. It was demonstrated that the antistatic paint plays a key role in inhibiting discharge activity. Once removed, discharges are initiated at the triple junction point which can lead to full flashover the test air gap when the applied voltage is sufficiently high. Such events cause significant erosion of the diverter strip end despite the lower magnitude of currents compared to those expected under lightning strikes.

ACKNOWLEDGEMENTS

The authors would like to thank Endeavr and AIRBUS Defense and Space Manching for the financial support.

REFERENCES

[1] C. Karch, C. Paul, and F. Heidler, "Lightning strike protection of radomes," presented at the 2019 Int. Symp. on Electromagnetic Compatibility, EMC EUROPE, Oct. 17, 2019, https://doi.org/10.1109/EMCEurope.2019.8871944.

[2] C. Karch, W. Wulbrand, and H. W. Zaglauer, "An approach to determining radome diverter strip geometry," vol. 2, presented at the Int. Conf. on Lightning and Electricity (ICOLSE), Blackpool, UK, 2003.

[3] C. Karch, W. Lick, and S. Pack, "Full-scale high voltage radome initial leader attachment tests," presented at the 2019 Int. Conf. on Lightning and Static Electricity, Wichita, KS, USA, 2019

[4] D. Yanchao, X. Xiu, and H. U. Pingdao, "Research on aircraft radome lightning protection based on segmented diverter strips," 2017 Int. Symp. on Electromagnetic Compatibility, EMC EUROPE, 2017, pp. 1–6, https://doi.org/10.1109/EMCEurope.2017.8094806

[5] J. A. Plumer and L. C. Hoots, "Lightning protection with segmented diverters," presented at the IEEE Int. Symp. On Electromagnetic Compatibility, Atlanta, GA, USA, 1978, https://doi.org/10.1109/ISEMC.1978.7566854.

[6] M. Banda, D. Malec, and J.-P. Cambronne, "Simulation of space charge impact on partial discharge inception voltage in power busbars dedicated to future hybrid aircrafts," Circ. Syst., vol. 9, no. 11, pp.196–212, 2018.

[7] Aircraft Lightning Test Methods, EUROCAE ED-105A, Jul. 2013.

[8] N. I. Petrov, A. Haddad, H. Griffiths, and R. T. Waters, "Lightning strikes to aircraft radome: Electric field shielding simulation," in Proc. 17th Int. Conf. on Gas Discharges and Their Applications, Sep. 8–11, 2008, pp. 513–516.

[9] H. Chen, F. Wang, X. Xiong, Z. He, and Z. Yue, "Plasma discharge characteristics of diverter strips subject to lightning strike," Plasma Sci. Technol., vol. 21, no. 2, p. 28, Nov. 2018.

[10] I. Gallimberti. "The mechanism of the long spark formation." J. Physique Colloques, vol. 40, no. c7, pp. c7-193–c7-250, 1979

[11] A. Bondiou and I. Gallimberti, "Theoretical modelling of the development of the positive spark in long gaps," J. Phys. D Appl. Phys., vol. 27, no. 6, pp. 1252–1266. https://doi.org/10.1088/0022-3727/27/6/024 , 1994.

[12] N. Goelian, P. Lalande, A. Bondiou-Clergerie, G. L. Bacchiega, A. Gazzani, and I. Gallimberti, "A simplified model for the simulation of positive-spark development in long air gap," J. Phys. D Appl. Phys., vol. 30, no. 17, pp. 2441–2452. https://doi.org/10.1088/0022-3727/30/17/010 , 1997.

[13] P. Lalande, V. Mazur, "A physical model of branching in upward leaders", AerospaceLab Journal, AL05-07, December 2012.

[14] Aircraft Lightning Environment and Related Test Waveforms Standards, EUROCAE ED-84, Jul. 2013.

[15] D. Morgan, C. J. Hardwick, S. J. Haigh, and A. J. Meakins, "The interaction of lightning with aircraft and the challenges of lightning testing," AerospaceLab J., no. 5, p. 1–10, 2012.

[16] Environmental Conditions and Test Procedures for Airborne Equipment—Lightning Direct Effects, EUROCAE ED-14E, Jul. 2013.

[17] K. C. Hsu, K. Etemadi, and E. Pfender, "Study of the free-burning high-intensity argon arc," J. Appl. Phys., vol. 54, no. 3, pp.1293–1301. https://doi.org/10.1063/1.332195, 1983.

[18] F. Lago, J. J. Gonzalez, P. Freton, and A. Gleizes, "A numerical modelling of an electric arc and its interaction with the anode: Part I. The two-dimensional model," J. Phys. D Appl. Phys., vol. 37, no. 6, p. 833. https://doi.org/10.1088/0022-3727/37/6/013, 2004.

[19] J. J. Gonzalez, F. Lago, P. Freton, M. Masquere, and X. Franceries, "Numerical modelling of an electric arc and its interaction with the anode: Part II. The three-dimensional model—Influence of external forces on the arc column," J. Phys. D Appl. Phys., vol. 38, no. 2, pp. 306–318. https://doi.org/10.1088/0022-3727/38/2/016, 2005.

[20] F. Wang, X. Ma, H. Chen, and Y. Zhang, "Evolution simulation of lightning discharge based on a magnetohydrodynamics method," Plasma Sci. Technol., vol. 20, no. 7, p. 075301. https://doi.org/10.1088/2058-6272/aab841, 2018

[21] M. Khalil, N. Abuelfoutouh, G. Abdelal, and A. Murphy, "Numerical simulation of lightning strike direct effects on aircraft skin composite laminate," Int. J. Architect. Environ. Eng., vol. 12, no. 2, pp. 173–186, 2018.

[22] G. Abdelal and A. Murphy, "A multiphysics simulation approach for efficient modeling of lightning strike tests on aircraft structures," IEEE Trans. Plasma Sci., vol. 45, no. 4, pp. 725–735, Apr.2017.

[23] F. Lago, J. J. Gonzalez, P. Freton, F. Uhlig, N. Lucius, and G. P. Piau, "A numerical modelling of an electric arc and its interaction with the anode: Part III. Application to the interaction of a lightning strike and an aircraft in flight," J. Phys. D Appl. Phys., vol. 39, no. 10, p. 2294. https://doi.org/10.1088/0022-3727/39/10/045, 2006.

[24] J. Pan, S. Hu, L. Yang, and S. Chen, "Numerical analysis of the heat transfer and material flow during keyhole plasma arc welding using a fully coupled tungsten–plasma–anode model," Acta Mater., vol. 118, pp. 221–229. https://doi.org/10.1016/j.actamat. 2016.07.046, 2016.

Federico Padoan joined Cardiff University in 2020, as a Research Associate. He received his B.S. and M.S. in energy and electrical engineering from Padua University, Italy. In the Advanced High Voltage Engineering Research Centre, he has been involved in projects to study the lightning interaction with aircraft structures and design the radar protection system. He is currently working on measurement systems for induced currents on high voltage lines.

David Clark (MIEEE) received the B.Eng. and Ph.D. degrees in electrical and electronic engineering from Cardiff University, Cardiff, U.K., in 2007 and 2012, respectively. He was a Research Associate in 2012, an Academic Post in 2014, with Cardiff University, where he is currently a Senior Lecturer of high voltage and high current engineering. His research interests include high-voltage insulation systems for aviation, lightning direct-effects, computational electromagnetics, and earthing in electrical energy systems.

A Haddad, FIET, FLSW, MIEEE, leads the Advanced High Voltage Engineering Research Centre. In 2004, he established a strategic partnership with National Grid. In 2011, he set up the Morgan-Botti Lightning Laboratory in collaboration with AIRBUS. He has published an IET textbook and over 300 papers, winning with co-researchers 14 paper prizes. Haddad is a member of several CIGRE working groups and Standards committees. He is now Chair of IEC-TC37 on overvoltage protection.

Christian Karch has been an Airbus Expert in Electromagnetics, Signature and Stealth since 2011. In 1993, he received his doctoral degree in Theoretical Solid-State Physics at University of Regensburg. From 1992 until 1996, he regularly visited the International School for Advanced Studies Trieste and the Institute Laue-Langevin Grenoble. From 1994 to 1997, he was a Teaching Assistant at Friedrich-Schiller University of Jena. Mr Karch co-authored more than 70 publications and more than 25 patent applications.

Peter Westphal manages the Global Research and Technology Cooperation's of Airbus Defence and Space GmbH. He is located in Munich, Germany. He held various Management positions within Airbus since 1995, including Strategy, Intellectual Property and Airworthiness / Flight Safety. He received the Dr.-Ing. degree "with distinction" appointments from the Technical University Munich. Topic: "Flight Control Systems and Flight Safety". He studied Aerospace Science at the Technical University Munich